(Received 12 May 2026, Accepted 18 June 2026, Scheduled 4 July 2026)

Performance Enhancement of a Dual-Core Photonic Crystal Fiber SPR Biosensor Using Hybrid Gold-TiO_2 Coatings

Riyadh Mwad Naife*

Biomedical Engineering Department, College of Engineering, University of Kerbala, Karbala, Iraq

ABSTRACT: A dual-core photonic crystal fiber (PCF) surface plasmon resonance (SPR) biosensor employing a hybrid Au-TiO_2 coating is presented for biosensing applications. This study was formulated as an extension of our earlier Au-only dual-core PCF-SPR design, where the main modification is the introduction of an ultra-thin TiO_2 dielectric overlayer to improve modal coupling and sensing response. The numerical analysis was carried out for analyte refractive indices from 1.28 to 1.44. A parametric analysis was also performed to examine the influence of the air-hole diameters, lattice pitch, and TiO_2-layer thickness on the resonance behavior and confinement-loss response. The results show a clear redshift in the resonance wavelength as the analyte refractive index increases, where the resonance wavelength shifts from 400 nm to 650 nm, corresponding to an overall wavelength shift of 250 nm across the investigated range. The confinement-loss spectra also show stronger coupling at higher refractive indices, with the largest loss peaks observed near the upper end of the sensing range. In addition, the amplitude sensitivity reaches a maximum absolute value of approximately 842 RIU^{-1}, confirming a strong intensity response around the resonance condition. Compared with the previous Au-only configuration, the hybrid Au-TiO_2 structure provides a measurable improvement in amplitude response and extends the usable lower-end refractive-index range. These results indicate that the proposed hybrid-coated dual-core PCF structure is a promising platform for high-contrast refractive-index detection.

1. INTRODUCTION

Surface plasmon resonance (SPR) sensing enables label-free monitoring of refractive-index (RI) variations at a metal-dielectric interface and is therefore attractive for biochemical, medical, and chemical diagnostics [1–5]. Photonic crystal fibers (PCFs) provide flexible microstructured geometries [6, 7] that can strongly confine light and support long interaction lengths, making PCF-based SPR sensors a highly sensitive platform [8–11]. Dual-core PCF structures are particularly attractive [12] because they support mode coupling between core-guided modes and supermodes, which can amplify loss resonances when the phase-matching condition with a surface plasmon polariton mode is satisfied [13, 14]. Recent studies have reported different PCF-SPR biosensor configurations for refractive-index and biomedical sensing applications, with continuous efforts directed toward improving sensitivity, resonance sharpness, modal coupling, and detection reliability. Recent reviews have also highlighted the importance of PCF-SPR and optical-fiber SPR biosensors for label-free biomedical detection, while optimization-based approaches have been used to improve sensor design with fewer simulation trials [15–17]. These developments show that the improvement of PCF-SPR biosensors is not limited to fiber geometry only, but also depends strongly on coating-layer engineering and resonance control.

Gold is a common plasmonic coating because of its chemical stability and well-established optical response; however, Au-only coatings can produce relatively broad resonance peaks, which may limit the detection resolution and reduce the figure of merit [2, 18, 19]. One practical strategy for improving the resonance quality is to engineer the coating stack by adding a thin high-index dielectric layer. Such a layer can modify the local optical environment, increase field overlap with the analyte, and improve spectral tuning [20–23].

In addition to geometry-based optimization, recent PCF-SPR studies have shown that sensing performance is strongly affected by plasmonic configuration, coating material, and modal-coupling condition. Rifat et al. [24] demonstrated a practical PCF-SPR configuration and reported wavelength- and amplitude-interrogation sensing characteristics. Wu et al. [3] showed that a side-polished gold-coated, hexagonal PCF can provide high wavelength sensitivity by increasing the accessibility of the guided field to the plasmonic interface. Recent comparison-oriented studies have also reported several advanced PCF-SPR configurations, including four-channel wide-range designs, twin-core D-shaped structures, hybrid Ag-TiO_2/Au-TiO_2 coated sensors, and D-type dual-mode PCF-SPR sensors with microfluidic channels [25–29]. These studies are included in the comparative evaluation because they represent different strategies for improving wavelength sensitivity, amplitude sensitivity, resonance tuning, and detection resolution. Other reported designs, including dual-core, microstructured, three-core, side-polished, and dual-plasmon-material PCF-SPR sensors [2, 11, 18, 22, 23], further confirm that both fiber architecture and coating-layer engineering play decisive roles in improving resonance shift, sensitivity, and detection resolution. Our earlier Au-only dual-core PCF-SPR sensor [1] was based on induced mode coupling in a gold-

* Corresponding author: Riyadh Mwad Naife (riyadh@uokerbala.edu.iq).

coated dual-core PCF structure. In the present work, the Au-only configuration is not repeated as a separate design, but is used as a baseline reference to quantify the effect of introducing the TiO_2 dielectric overlayer. Therefore, the contribution of the present study is reformulated as a hybrid-coating and modal-coupling enhancement study, where an Au-TiO_2 bilayer is used to tune the plasmonic interface, improve the analyte-field interaction, and extend the usable refractive-index sensing range. Accordingly, the present manuscript focuses on resonance tunability, expanded sensing metrics, and comparative performance evaluation of the proposed hybrid Au-TiO_2 coated dual-core PCF-SPR biosensor.

2. SENSOR STRUCTURE AND NUMERICAL METHOD

2.1. Sensor Configuration

Figure 1 presents the cross-sectional schematic of the proposed PCF-SPR sensor employed in this study. The modeled structure is formed in a fused-silica background and consists of a hexagonal lattice of circular air holes with two distinct diameters. The smaller and larger air holes are characterized by $d_1 = 0.4\,\mu m$ and $d_2 = 0.8\,\mu m$, respectively, while the pitch is fixed at $\Lambda = 1.2\,\mu m$. The use of two different air-hole diameters is intended to tailor the modal confinement and enhance the interaction between the guided core mode and the plasmonic sensing interface.

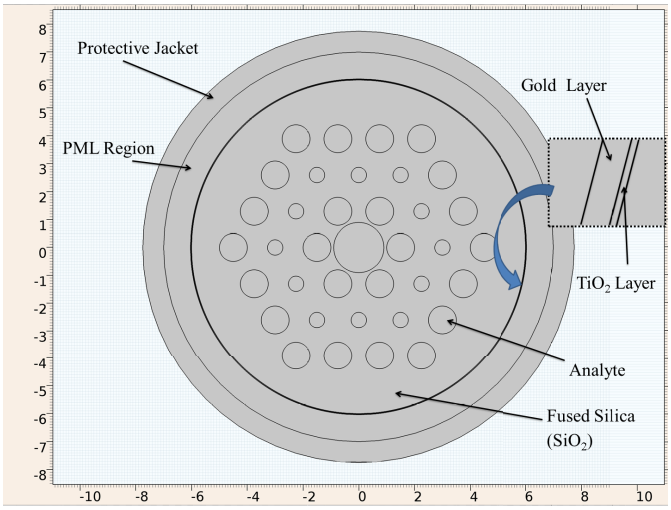

FIGURE 1. Schematic representation of the cross-sectional structure of the proposed PCF-SPR biosensor.

The sensing region is defined at the plasmonic interface adjacent to the central modified region of the fiber. In this region, a thin Au layer is introduced as the primary SPR-active metal layer, followed by an ultra-thin TiO_2 dielectric overlayer deposited on the outer side of the Au film. The analyte is assigned to the region in contact with the outer TiO_2 surface, so that changes in the analyte refractive index directly modify the optical environment of the plasmonic interface. This description clarifies that the analyte region is the sensing medium adjacent to the coated interface and should not be confused with the structural air holes of the PCF.

Following the general architecture established in our earlier Au-only design [1], the present work preserves the same basic sensing platform while introducing a TiO_2 overlayer as an additional high-index dielectric layer. This hybrid bilayer arrangement is adopted to isolate the effect of the TiO_2 overlayer on mode-coupling behavior and sensor performance while preserving the same basic sensing platform.

Although the present study is numerical, the proposed structure is considered a feasible direction for future experimental implementation. The fabrication of cylindrical metal-coated PCF-SPR structures is more challenging than that of side-polished or D-shaped fibers because precise deposition of plasmonic and dielectric layers around microstructured regions requires careful control. Possible fabrication routes may include PCF drawing followed by selective infiltration of the sensing region and subsequent deposition of the Au and TiO_2 layers using controlled thin-film coating techniques. Therefore, the proposed design is intended to provide a numerically investigated platform that can guide future experimental realization of hybrid-coated PCF-SPR sensors. For clarity and reproducibility, the structural parameters used in the final refractive-index sensing simulations are summarized in Table 1. These values represent the adopted simulation configuration used for the sensing analysis. The parametric study was then used to examine how variations in each parameter affect the resonance and confinement-loss behavior, rather than to claim a global optimum.

TABLE 1. Final selected structural parameters used in the sensing simulations of the proposed hybrid Au-TiO_2-coated dual-core PCF-SPR biosensor.

Parameter	Value
Smaller air-hole diameter, d_1	0.4 μm
Larger air-hole diameter, d_2	0.8 μm
Lattice pitch, Λ	1.2 μm
Au layer thickness	40 nm
TiO_2 overlayer thickness	5 nm

2.2. Material Modeling

In the numerical analysis, the optical properties of the constituent materials were modeled as wavelength-dependent in order to accurately describe the propagation, modal coupling, and plasmonic resonance behaviors over the investigated spectral range. The background material of the photonic crystal fiber was assumed to be fused silica, whose refractive index was calculated using the Sellmeier dispersion relation commonly used in PCF modeling [9, 30]. For silica, the refractive index is commonly expressed as:

$$n^2_{SiO_2}(\lambda) - 1 = \frac{0.6961663\lambda^2}{\lambda^2 - (0.0684043)^2} + \frac{0.4079426\lambda^2}{\lambda^2 - (0.1162414)^2} + \frac{0.8974794\,\lambda^2}{\lambda^2 - (9.896161)^2} \quad (1)$$

where λ is the operating wavelength in μm, and this Sellmeier model is widely used for fused silica and is valid over

the optical range relevant to the PCF-SPR analysis. The plasmonic layer was assumed to be gold because of its chemical stability and well-established performance in SPR-based optical sensors [4, 8]. The Au layer was modeled as a dispersive lossy metal using wavelength-dependent complex optical constants. The complex refractive index of gold, $(n_{\mathrm{Au}} + ik_{\mathrm{Au}})$, was taken in accordance with the widely used Johnson-Christy dataset [13], which covers the visible and near-infrared spectral range relevant to plasmonic analysis. The complex permittivity of gold was obtained from:

$$\varepsilon_{\mathrm{Au}}(\lambda) = [n_{\mathrm{Au}}(\lambda) + ik_{\mathrm{Au}}(\lambda)]^2 \tag{2}$$

$$\varepsilon_{\mathrm{Au}} = \varepsilon_r + i\varepsilon_i \tag{3}$$

where ε_r and ε_i are the real and imaginary parts of the dielectric function, respectively. This treatment accounts for both the negative real permittivity required for plasmon excitation and the intrinsic absorption loss of the metal layer.

For the hybrid coating, the TiO_2 overlayer was also described using a wavelength-dependent refractive index. In the present model, the refractive index of rutile TiO_2 was calculated using the DeVore dispersion relation [31]:

$$n^2_{\mathrm{TiO_2}}(\lambda) = 5.913 + \frac{0.2441}{\lambda^2 - 0.0803} \tag{4}$$

with λ in μm. This model was employed within the same spectral window used for the sensing analysis. In the present work, the main physical role of the TiO_2 overlayer is not simply its dispersive nature, since all main materials are treated as wavelength-dependent, but rather its relatively high refractive index compared with the surrounding sensing medium. The TiO_2 layer modifies the local optical environment at the Au-dielectric interface, shifts the plasmonic phase-matching condition, and alters the coupling strength between the guided core mode and the surface plasmon mode [15, 27, 28].

Because TiO_2 is commonly treated as a low-loss dielectric in simplified PCF-SPR models over the investigated optical range, its extinction coefficient was neglected in the present analysis [27, 28, 31]. This approximation allows the effect of the high-index dielectric overlayer on modal coupling and resonance tuning to be isolated. For experimentally deposited thin films, however, a more detailed model may use measured complex optical constants of TiO_2, especially when film absorption, deposition conditions, or nanoscale thickness variations are considered [31].

Overall, fused silica, Au, and TiO_2 were all modeled using wavelength-dependent optical properties. This ensures that the calculated effective index, confinement loss, resonance wavelength, and sensing response reflect the dispersive behavior of the proposed hybrid Au-TiO_2-coated PCF-SPR biosensor within the actual operating wavelength range considered in this study.

2.3. FEM Simulation Settings

The modal characteristics of the proposed sensor were analyzed using a finite element method (FEM)-based eigenmode solver, which was employed to calculate the complex effective refractive indices of the guided and plasmonic modes supported by the structure. The real part of the effective index provides information on mode propagation, whereas the imaginary part is related to modal attenuation and was used to evaluate the confinement-loss response.

To emulate an open computational domain and avoid artificial reflections from the simulation boundary, perfectly matched layers (PMLs) were imposed at the outer boundary of the model. Local mesh refinement was applied near the Au and TiO_2 coating regions, where the electromagnetic field exhibits strong spatial variation due to plasmonic excitation. The mesh was refined until the calculated effective index and resonance position showed stable behavior with negligible variation upon further refinement. This procedure ensured that the reported confinement-loss spectra and resonance wavelengths were not significantly affected by numerical discretization.

2.4. Performance Metrics

The sensing characteristics of the proposed PCF-SPR biosensor were evaluated using standard SPR performance metrics, including confinement loss, resonance-wavelength shift, wavelength sensitivity, average wavelength sensitivity, amplitude sensitivity, sensor resolution, full width at half maximum (FWHM), and figure of merit (FOM). The confinement loss was obtained from the imaginary part of the complex effective refractive index of the guided mode as follows [9, 24]:

$$L_c = 8.686 \times \left(\frac{2\pi}{\lambda}\right) \times \mathrm{Im}(n_{\mathrm{eff}}) \times 10^4 \tag{5}$$

where λ is the operating wavelength in micrometers; $\mathrm{Im}(n_{\mathrm{eff}})$ is the imaginary part of the effective refractive index; and L_c is expressed in dB/cm. The resonance wavelength λ_{res} was identified from the maximum value of the confinement-loss peak for each analyte refractive index.

The wavelength sensitivity was calculated from the displacement of the resonance wavelength caused by a change in the analyte refractive index [3, 24]:

$$S_\lambda = \frac{\Delta\lambda_{\mathrm{res}}}{\Delta n_a} \tag{6}$$

where $\Delta\lambda_{\mathrm{res}}$ is the resonance-wavelength shift, and Δn_a is the corresponding analyte refractive-index variation. To compare the overall spectral response across the full sensing range, the average wavelength sensitivity was calculated as:

$$S_{\lambda,\mathrm{avg}} = \frac{\lambda_{\mathrm{res,max}} - \lambda_{\mathrm{res,min}}}{n_{a,\mathrm{max}} - n_{a,\mathrm{min}}} \tag{7}$$

where $\lambda_{\mathrm{res,max}}$ and $\lambda_{\mathrm{res,min}}$ are the resonance wavelengths corresponding to the maximum and minimum analyte refractive indices, respectively, while $n_{a,\mathrm{max}}$ and $n_{a,\mathrm{min}}$ are the maximum and minimum analyte refractive indices considered in the sensing range.

The amplitude sensitivity was obtained from the normalized variation of confinement loss with respect to the analyte refractive index [2, 24]:

$$S_A(\lambda) = -\frac{1}{\alpha(\lambda, n_a)} \frac{\partial\alpha(\lambda, n_a)}{\partial n_a} \tag{8}$$

where $\alpha(\lambda, n_a)$ is the confinement loss at wavelength λ and analyte refractive index n_a. In the numerical analysis, the derivative can be evaluated using a finite-difference approximation:

$$S_A(\lambda) \approx -\frac{1}{\alpha(\lambda, n_a)} \frac{\alpha(\lambda, n_a + \Delta n_a) - \alpha(\lambda, n_a)}{\Delta n_a} \quad (9)$$

The sign of S_A indicates the direction of loss variation; therefore, the absolute value $|S_A|$ was used when the maximum amplitude sensitivities of different sensors are compared.

The sensor resolution was estimated using the minimum detectable wavelength shift of the interrogation system [3, 25, 26]:

$$R = \frac{\Delta n_a \times \Delta\lambda_{\text{min}}}{\Delta\lambda_{\text{res}}} \quad (10)$$

where $\Delta\lambda_{\text{min}}$ is the minimum measurable spectral shift. In this work, $\Delta\lambda_{\text{min}} = 0.1$ nm was adopted, which is commonly used in numerical evaluations of PCF-SPR sensors.

The resonance linewidth was represented by the full width at half maximum (FWHM) of the confinement-loss peak. The figure of merit was then calculated as [26, 28]:

$$\text{FOM} = \frac{S_\lambda}{\text{FWHM}} \quad (11)$$

A smaller FWHM and a larger wavelength sensitivity lead to a higher FOM, indicating sharper resonance and better spectral detection capability. The inclusion of these metrics provides a more complete assessment of the proposed sensor than confinement loss and amplitude sensitivity alone.

3. PARAMETRIC STUDY PLAN

To ensure a fair and physically meaningful comparison between the conventional gold-coated structure and the proposed hybrid Au-TiO_2 configuration, the geometrical parameters of the PCF were kept unchanged throughout the analysis. First, the Au-only design reported in our previous work [1] was used as the baseline reference structure. Then, a thin TiO_2 overlayer was introduced above the Au film to investigate its influence on the sensing characteristics of the sensor. Thus, the observed performance difference can be attributed primarily to the added dielectric overlayer rather than to a change in the underlying fiber architecture. In the parametric study, the gold thickness and analyte refractive index were varied systematically within selected ranges. For each parameter set, the confinement loss spectrum was calculated over the wavelength range of interest. The resonance behavior was identified from the loss peak, and the corresponding amplitude sensitivity was evaluated to determine the effect of each parameter on the sensor performance.

4. RESULTS AND DISCUSSION

4.1. Comparative Mode Coupling and Loss Characteristics

To demonstrate the effect of the proposed dielectric-assisted coating, the performance of the present hybrid design was compared with that of the previously reported Au-only structure from our earlier study [1]. Fig. 2 summarizes this comparison in terms of the modal characteristics and the corresponding confinement-loss spectra. As shown in Fig. 2(a), the real part of the effective refractive index of the interacting modes in the proposed hybrid structure reveals phase-matching regions between the fundamental and plasmonic modes. These coupling wavelengths are indicated by the dashed vertical lines. Fig. 2(b) highlights the corresponding mode-interaction behavior used as a reference for the conventional Au-coated design. In Fig. 2(c), the confinement-loss spectra of the Au-only and Au + TiO_2 configurations are compared directly. It is evident that the introduction of the TiO_2 overlayer modifies both the resonance wavelength and the peak-loss magnitude. The resonance peaks of the hybrid structure were shifted relative to those of the Au-only configuration, and their amplitudes were altered, indicating a change in the modal coupling condition at the metal-dielectric interface. These results confirm that the dielectric overlayer provides an effective means of tuning the plasmonic response and support the interpretation of the present work as a materials-level development of the previous Au-only sensor platform.

The role of the TiO_2 overlayer can therefore be understood as a modification of the optical environment surrounding the plasmonic interface. Since TiO_2 has a higher refractive index than the surrounding analyte region, its incorporation above the gold layer changes the effective index of the plasmonic mode and shifts the phase-matching condition with the guided core mode. This modification enhances the overlap between the guided field and the plasmonic sensing region, leading to a stronger resonance response. Accordingly, the hybrid Au-TiO_2 coating provides an additional degree of freedom for tuning the resonance wavelength and improving the sensing performance compared with the Au-only configuration. The vertical dashed lines in Fig. 2 are used as visual guides to show the relationship between the mode-interaction regions in Figs. 2(a), (b) and the loss peaks in Fig. 2(c). When the effective indices of the guided core mode and the plasmonic mode become close to each other, phase matching occurs, and the coupling between the two modes becomes stronger. This stronger coupling transfers optical energy toward the plasmonic sensing interface, which leads to the resonance-loss peaks. Therefore, the dashed lines confirm that the observed loss peaks are produced by modal coupling rather than by random spectral variations.

4.2. Field Distribution and Mode Interaction Analysis

To gain deeper physical insight into the sensing mechanism of the proposed PCF-SPR structure, the electric-field distributions of the main interacting modes were investigated. These field profiles clearly show that the resonance behavior originates from the interaction between the core-guided fundamental and plasmonic modes supported at the metal-dielectric interface. As shown in Fig. 3(a), the fundamental mode (FM) is mainly confined within the central core region. Most of the optical energy remains concentrated in the fiber core, while only a weak evanescent tail extends toward the surrounding plasmonic region. This distribution indicates that the overlap between the guided field and the sensing interface is still limited,

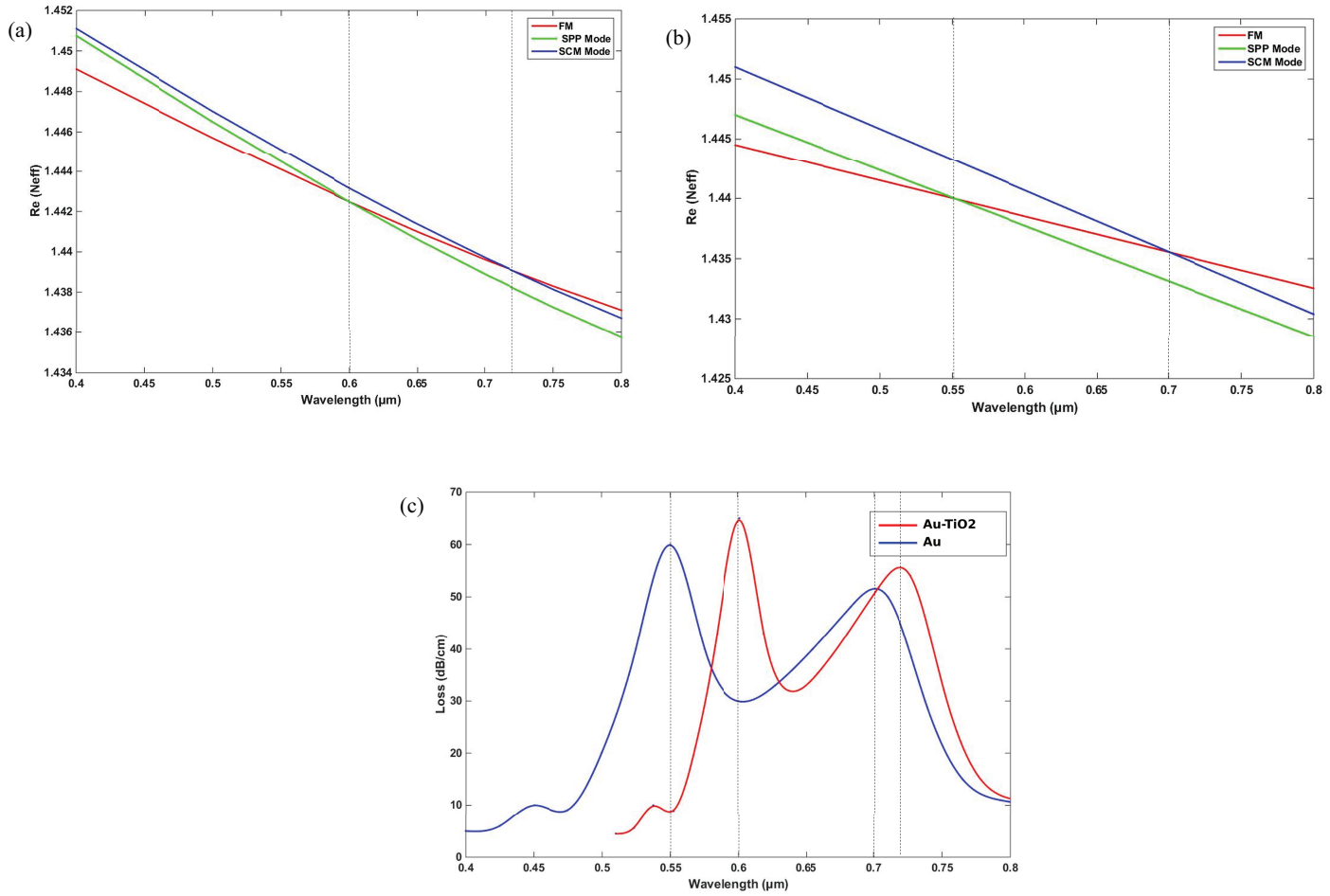

FIGURE 2. Real part of the effective refractive index for the fundamental mode, SPP mode, and SCM mode under different coating configurations: (a) hybrid Au-TiO_2-coated structure and (b) Au-only coated structure. (c) Corresponding confinement-loss spectra for the hybrid Au-TiO_2 and Au-only coatings. In (c), the red curve represents the hybrid Au-TiO_2 coating, while the blue curve represents the Au-only coating. The dashed vertical lines are added as visual guides to correlate the modal intersection/phase-matching points in (a) and (b) with the resonance-loss peaks in (c), confirming that each loss peak originates from enhanced coupling between the guided core mode and the plasmonic mode.

and therefore no strong coupling occurs under this condition. In Fig. 3(b), the surface plasmon polariton mode (SPP mode) exhibits a markedly different field distribution. In this case, the optical field becomes strongly localized near the plasmonic interface, indicating that the modal energy is concentrated around the coated sensing region rather than inside the core. This behavior confirms the plasmonic nature of the mode and reflects its strong dependence on the metal-dielectric boundary. The field pattern presented in Fig. 3(c) corresponds to the SCM mode, which represents a hybridized modal state. Unlike the FM and SPP modes, the field in this case is neither fully confined in the core nor entirely localized at the plasmonic interface. Instead, it shows a redistributed profile, indicating stronger interaction and energy exchange between the guided and plasmonic modes. This mixed field behavior is a clear signature of modal hybridization near the phase-matching condition. The paired field profiles shown in Fig. 3(d) and Fig. 3(e) further illustrate the field evolution during the coupling process. In one case, the field remains more concentrated around the core region, indicating stronger core-guided characteristics. In the other, a significant portion of the optical energy is transferred toward the annular plasmonic region, which reflects stronger coupling with the sensing interface. This gradual redistribution of modal energy confirms that resonance is established through coupling between the interacting modes rather than through an isolated modal state. Similarly, Fig. 3(f) and Fig. 3(g) demonstrate the transition between the resonance-associated state and the fundamental guided state. One distribution shows enhanced localization near the plasmonic region, while the other preserves stronger confinement at the fiber center. The coexistence of these two patterns near the same spectral region indicates that the interacting modes become strongly mixed around the phase-matching wavelength. Overall, these field distributions provide clear physical evidence that the confinement-loss peaks observed in the spectral response are directly associated with coupling between the fundamental core mode and the plasmonic mode. When the optical field remains largely confined in the core, the interaction with the metal-dielectric interface is weak, and the confinement loss stays relatively low. However, when the field extends sig-

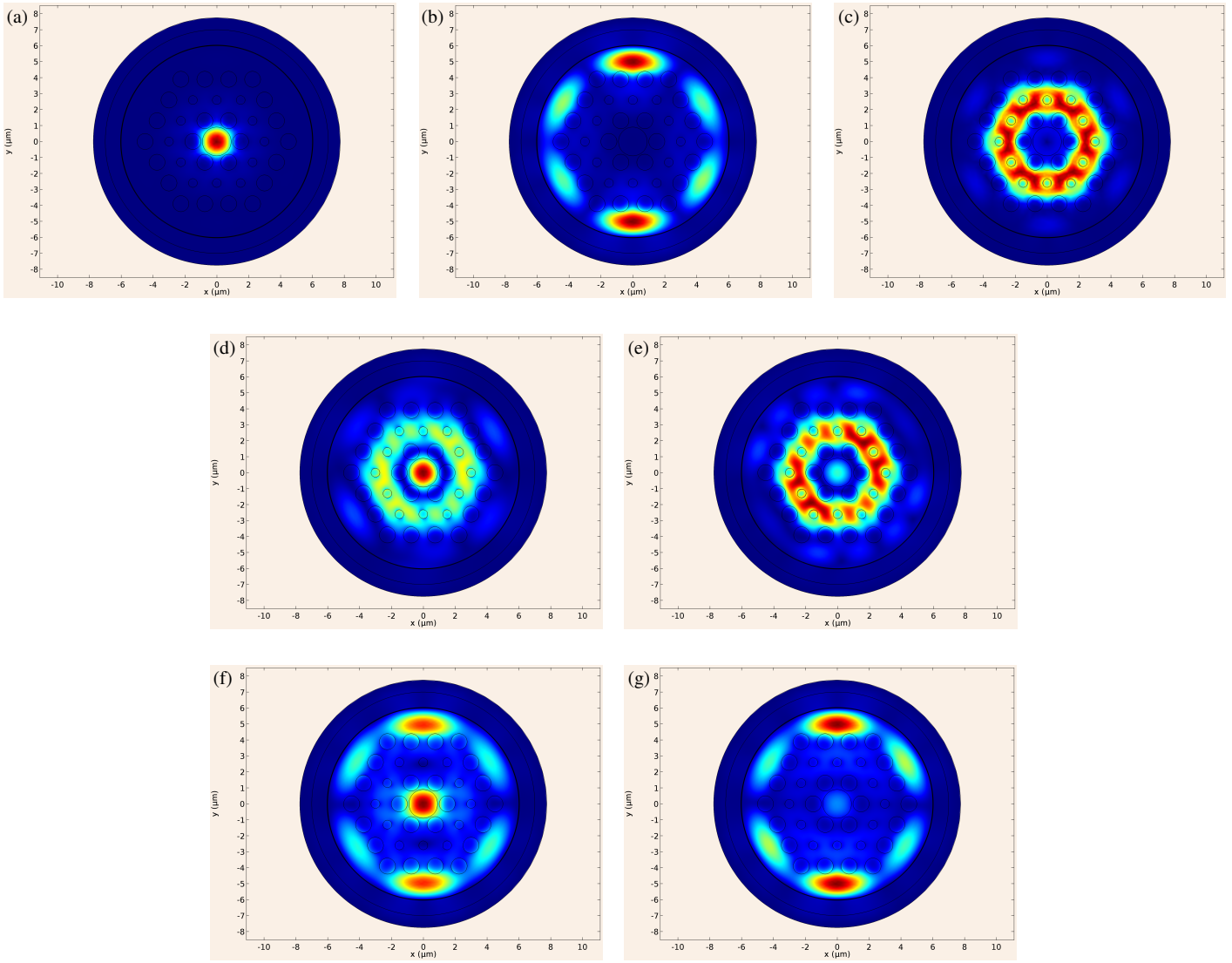

FIGURE 3. Representative mode profiles of the proposed PCF-SPR sensor. Panels (a)–(c) correspond to non-resonant conditions, where no strong modal interaction is observed. Panels (d) and (e) show the interaction between the cladding mode and the fundamental mode, while panels (f) and (g) show the interaction between the resonant mode and the fundamental mode.

nificantly toward the coated sensing region, the modal overlap increases, leading to stronger plasmonic coupling and consequently higher confinement loss.

4.3. Parametric Analysis of the Proposed Sensor

To further evaluate the performance of the proposed hybrid PCF-SPR biosensor, a parametric analysis was performed by varying selected structural parameters while keeping the remaining geometrical and material properties unchanged. This analysis is important for identifying the parameter values that provide a stronger plasmonic coupling and improved sensing behavior. Among the investigated parameters, diameter d_1 plays a significant role in controlling the field distribution inside the fiber and the overlap between the guided mode and the plasmonic sensing interface. Therefore, the effect of varying d_1 on the confinement-loss spectrum was first examined. Fig. 4 illustrates the effect of d_1 on the confinement-loss response of the proposed sensor. The resonance peaks are strongly influenced by this parameter. As d_1 increased from 0.2 μm to 0.4 μm, the peak loss values increased significantly, and the resonance wavelengths shifted accordingly. The strongest resonance is obtained at $d_1 = 0.4$ μm, indicating improved coupling between the guided and plasmonic modes. It suggests that d_1 is a key parameter in tuning the spectral response of the sensor. This behavior indicates that increasing d_1 improves the interaction between the guided field and the sensing region. Therefore, the increase in peak loss not only is a change in magnitude, but also reflects a stronger resonance condition.

Figure 5 shows the effect of varying the structural parameter d_2 on the confinement-loss spectrum of the proposed PCF-SPR sensor. In this analysis, d_2 was changed from 0.8 μm to 1.0 μm, while the remaining geometrical and material parameters were kept unchanged. It is evident that the confinement-loss response is highly sensitive to this parameter because both

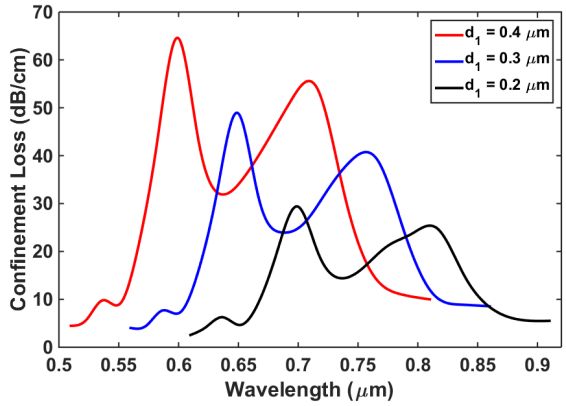

FIGURE 4. Confinement-loss spectra of the proposed PCF-SPR sensor as a function of wavelength for three selected values of d_1. Each accompanying mode profile corresponds to one of the selected d_1 values.

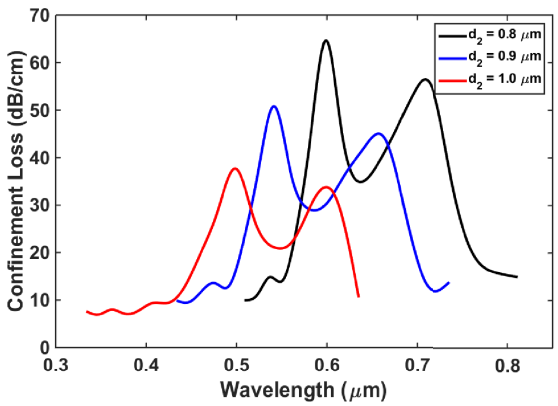

FIGURE 5. Confinement-loss spectra of the proposed PCF-SPR sensor as a function of wavelength for three selected values of d_2. Each accompanying mode profile corresponds to one of the selected d_2 values.

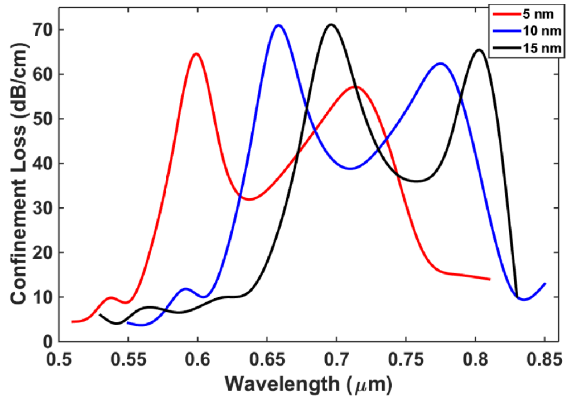

FIGURE 6. Effect of TiO_2 layer thickness on the confinement-loss spectrum of the proposed hybrid PCF-SPR sensor. Each accompanying mode profile corresponds to one of the selected TiO_2 thickness values.

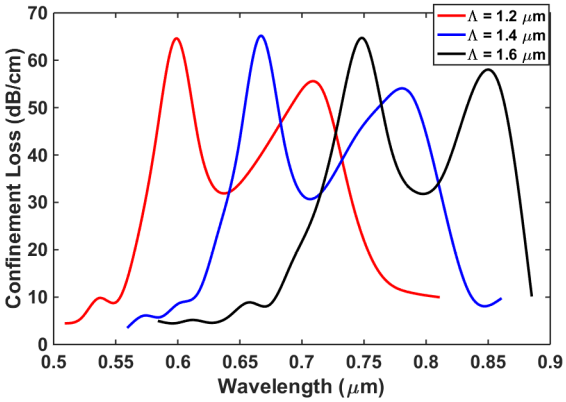

FIGURE 7. Effect of pitch Λ on the confinement-loss spectrum of the proposed hybrid PCF-SPR sensor. Each accompanying mode profile corresponds to one of the selected pitch values.

the resonance wavelength and the peak loss magnitude varied significantly with changing d_2. For $d_2 = 0.8\,\mu$m, the loss spectrum exhibits the strongest resonance behavior, with pronounced peaks appearing in the longer-wavelength region and the maximum confinement loss reaching approximately 65 dB/cm. This indicates that the modal coupling between the guided core mode and the plasmonic mode becomes stronger at this diameter. When d_2 is increased to 0.9 µm, the resonance peaks shift and their amplitudes decrease compared with the previous case, showing a moderate coupling condition. A further increase to $d_2 = 1.0\,\mu$m results in a clear reduction in the loss magnitude, with weaker and less pronounced resonance peaks, suggesting a lower overlap between the guided field and plasmonic sensing interface. This behavior can be attributed to the role of d_2 in modifying the field confinement and phase-matching condition inside the fiber structure. Changing this diameter affects the spatial distribution of the guided mode and its evanescent extension toward the metal-dielectric region of the fiber. Consequently, the strength of plasmonic coupling is altered, which is directly reflected in the confinement-loss spectrum. Based on the obtained results, the case of $d_2 = 0.8\,\mu$m provides the strongest resonance response among the examined values and can therefore be considered the most favorable choice for this parameter.

Figure 6 illustrates the effect of varying the TiO_2 dielectric-layer thickness on the confinement-loss spectrum of the proposed sensor. Three thickness values, namely 5 nm, 10 nm, and 15 nm, were considered while keeping the other parameters fixed. It is evident that changing the TiO_2 thickness leads to noticeable shifts in the resonance peaks and variations in the peak-loss values. The thicker TiO_2 layers of 10 nm and 15 nm produce stronger and more pronounced resonance peaks than the 5 nm layer, indicating that the dielectric overlayer thickness has a clear influence on the plasmonic coupling condition.

This result shows that the TiO_2 thickness can be used as an effective tuning parameter for controlling the resonant response. However, in the final refractive-index sensing analysis, the 5 nm TiO_2 overlayer was retained as the adopted ultra-thin dielectric coating in order to evaluate the effect of the minimal TiO_2 modification on the original Au-only dual-core platform. Therefore, the 5 nm value should be understood as the adopted simulation thickness used for the comparative sensing analysis, not as the globally optimal TiO_2 thickness.

Figure 7 shows the effect of changing the pitch Λ on the confinement-loss spectrum of the proposed sensor. Three pitch

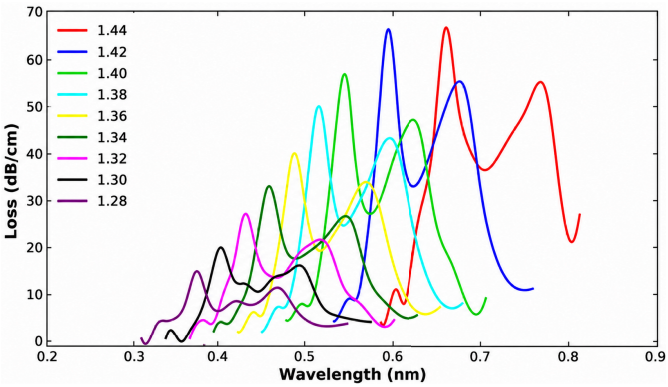

FIGURE 8. Effect of analyte refractive index on the confinement-loss spectrum of the proposed hybrid PCF-SPR sensor.

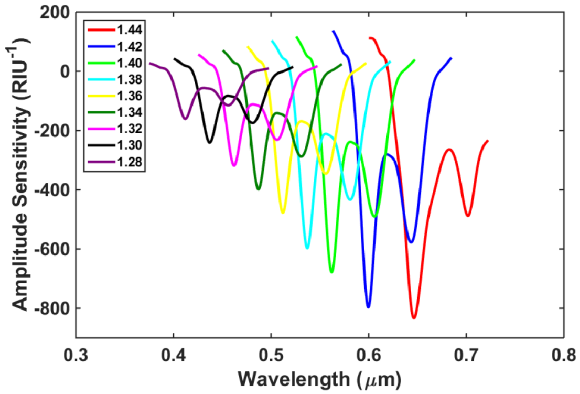

FIGURE 9. Effect of analyte refractive index on the amplitude sensitivity of the proposed hybrid PCF-SPR sensor.

values of 1.2 µm, 1.4 µm, and 1.6 µm, were examined while keeping the other parameters unchanged. It is observed that varying Λ causes clear shifts in the resonance peaks and significant changes in the loss magnitude. As the pitch increasesed, the resonance peaks moved toward shorter wavelengths, accompanied by a modification in the peak intensity. This indicates that the pitch has a significant influence on the modal confinement and coupling condition between the guided and plasmonic modes. Therefore, Λ can be considered an important parameter for tuning the spectral response of the proposed hybrid PCF-SPR sensor. This trend shows that the pitch mainly controls the spacing between the air holes and hence the degree of field confinement in the core region. As a result, small variations in Λ can noticeably change the resonance position and the loss amplitude.

4.4. Amplitude Sensitivity Characteristics

To further evaluate the sensing performance of the proposed hybrid PCF-SPR sensor, the confinement-loss spectra, amplitude sensitivity, and resonance-wavelength shift were analyzed for different analyte refractive indices. These results provide a comprehensive view of the spectral evolution, strength of amplitude-based interrogation, and overall wavelength response of the proposed structure. Although Fig. 8 presents the confinement-loss behavior, it is discussed in this section because the amplitude-sensitivity response is closely related to the variation of confinement loss with analyte refractive index. Therefore, presenting the confinement-loss behavior together with the amplitude-sensitivity results helps clarify how changes in the loss spectrum influence the sensitivity response. As shown in Fig. 8, the confinement-loss spectra shift progressively toward longer wavelengths as the analyte refractive index increased from 1.28 to 1.44. This redshift indicates that the phase-matching condition between the guided and plasmonic modes occurs at higher wavelengths for larger analyte refractive indices. In addition, the resonance peaks became stronger at higher refractive-index values, particularly for $na = 1.42$ and 1.44, confirming enhanced plasmonic coupling in this range.

The corresponding amplitude-sensitivity response is shown in Fig. 9. The amplitude-sensitivity curves are mainly negative around the resonance region, indicating a rapid decrease in the confinement loss with the refractive-index variation at the selected wavelengths. In practical amplitude-interrogation sensing, the absolute magnitude is more important than the sign. The highest absolute amplitude sensitivity is obtained at higher analyte refractive indices, reaching approximately 842 RIU^{-1} for $na = 1.44$ followed by approximately 818 RIU^{-1} for $na = 1.42$. This behavior confirms that the amplitude-sensitivity response becomes stronger at the upper end of the investigated refractive-index range. It should be noted that the maximum amplitude sensitivity reported here is extracted from the wavelength-dependent amplitude-sensitivity spectrum and should not be interpreted as a fixed-wavelength operating sensitivity. In practical sensing operation, the proposed sensor is mainly calibrated using the resonance-wavelength shift with analyte refractive index, while the amplitude-sensitivity spectrum provides an additional metric for describing the RI-dependent loss variation near the resonance region.

Figure 10 summarizes the variation in the resonance wavelength with the analyte refractive index. A clear monotonic increase in the resonance wavelength was observed as the analyte refractive index increased, confirming the redshifting behavior observed in the loss spectra. This trend demonstrates that the proposed sensor provides a stable spectral response over the examined refractive-index range and supports its applicability for refractive-index sensing. The wavelength-interrogation re-

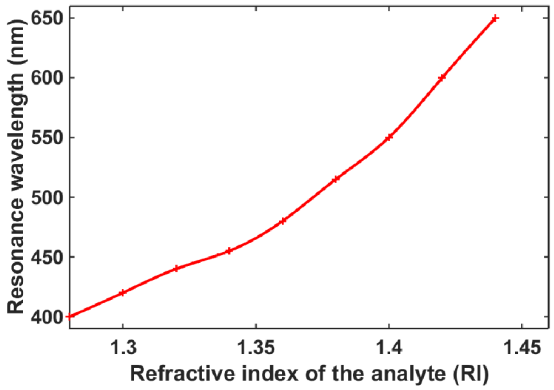

FIGURE 10. Resonance wavelength as a function of analyte refractive index for the proposed hybrid PCF-SPR sensor.

TABLE 2. Performance comparison of the proposed hybrid Au-TiO_2 coated dual-core PCF-SPR biosensor with selected reported PCF-SPR sensors.

Ref.	Sensor configuration	Plasmonic layer	Operating/resonance window	RI range	Max. S_λ (nm/RIU)	Avg. S_λ (nm/RIU)	Max. $\lvert S_A \rvert$ (RIU^{-1})	Resolution (RIU)
[3]	Gold-coated side-polished hexagonal PCF-SPR biosensor	Au	∼1.1–1.5 μm	1.33–1.34	21700	∼21700	NR	$\sim 4.61 \times 10^{-6}$
[24]	External-sensing practical PCF-SPR biosensor	Au	∼0.60–0.70 μm	∼1.33–1.37	4000	∼4000	320	2.50×10^{-5}
[25]	Four-channel PCF-SPR biosensor with wide sensing range	Au/Au–Ta_2O_5	Visible–near-IR	1.30–1.41	25000	∼18000	803.827	$\sim 4.00 \times 10^{-6}$
[26]	Twin-core gold-coated D-shaped PCF-SPR sensor	Au	Near-IR resonance region	1.28–1.42	9000	∼9000	3746	1.00×10^{-5}
[27]	PCF-SPR biosensor coated with Ag–TiO_2 and Au–TiO_2 for skin-cancer detection	Ag–TiO_2 / Au–TiO_2	Visible / biological sensing window	Cancer-cell RI range	NR	NR	NR	NR
[28]	D-type dual-mode PCF-SPR RI sensor with microfluidic channel	Au–TiO_2	Visible–near-IR	1.25–1.36	33000	8272.7	NR	NR
[1]	Previous Au-only dual-core PCF-SPR sensor	Au	∼1.2–1.8 μm	1.30–1.44	∼25000	∼1500–2000	700	$\sim 4.00 \times 10^{-6}$
This work	Hybrid Au–TiO_2 coated dual-core PCF-SPR biosensor with structural-parameter tuning	Au–TiO_2	0.4–0.8 μm	1.28–1.44	∼30600	∼1562.5	∼842	$\sim 3.27 \times 10^{-6}$

WS: wavelength sensitivity; AS: amplitude sensitivity; RI: refractive index; NR: not reported or not safely available from the cited source. The symbol "∼" indicates values calculated approximately from reported resonance-shift data, estimated from plotted spectra, or inferred from the available comparison information. For the present work, the wavelength-sensitivity values were extracted from the resonance-wavelength calibration and included to support wavelength-interrogation performance evaluation. The estimated resolution was calculated using $R = \Delta n_a \Delta\lambda_{\min}/\Delta\lambda_{\text{res}}$ with $\Delta\lambda_{\min} = 0.1$ nm when the required wavelength-shift information was available.

sponse was evaluated from the resonance-wavelength shift with respect to the analyte refractive-index variation according to $S_\lambda = \Delta\lambda_{\text{res}}/\Delta n_a$. Based on the resonance-wavelength calibration shown in Fig. 10, the maximum and average wavelength sensitivities were extracted and included among the main sensing-performance metrics. These results complement the amplitude-sensitivity analysis and provide a more complete evaluation of the proposed hybrid Au-TiO_2-coated PCF-SPR biosensor.

To further evaluate the resonance quality of the proposed sensor, the figure of merit was considered in relation to the resonance linewidth. The FOM is commonly defined as the ratio between the wavelength sensitivity and the full-width at half maximum of the resonance peak, i.e., FOM $= S_\lambda/FWHM$. A higher FOM indicates a sharper resonant response and better wavelength-discrimination capability. Therefore, FOM provides a useful complementary metric together with wavelength sensitivity, amplitude sensitivity, and resolution.

To quantify the quality of the calibration fitting in Fig. 10, a second-order polynomial fitting was applied to the extracted resonance-wavelength data. The obtained fitting parameters were $R^2 = 0.9979$, SSE $= 123.10$, and MSE $= 13.68$, indicating good agreement between the fitted calibration curve and the extracted resonance-wavelength data.

4.5. Comparative Performance Evaluation

To clarify the relative performance of the proposed hybrid Au-TiO_2-coated dual-core PCF-SPR biosensor, a broader comparative evaluation was carried out with selected reported PCF-SPR sensors. The comparison was expanded beyond the authors' previous Au-only dual-core structure and includes different sensing configurations, such as practical external-sensing PCF-SPR structures, side-polished gold-coated PCFs, four-channel plasmonic PCF sensors, twin-core D-shaped PCF-SPR sensors, skin-cancer-oriented hybrid-coated PCF-SPR sensors, and D-type dual-mode PCF-SPR sensors with microfluidic channels. The earlier Au-only dual-core PCF-SPR sensor reported in the ARPN Journal of Engineering and Applied Sciences [1] is retained only as a baseline reference, because the present structure is developed on the same sensing platform. Therefore, the comparison is not limited to the authors' previous work, but places the proposed hybrid Au-TiO_2 design within the wider PCF-SPR literature and recent state-of-the-art sensing strategies.

The comparison was based on the plasmonic layer, operating or resonance window, analyte refractive-index range, maximum wavelength sensitivity, average wavelength sensitivity, maximum amplitude sensitivity, and estimated resolution. The results are summarized in Table 2. When exact values were not explicitly stated in the cited works, approximate values were estimated from the reported resonance shifts, available sensing ranges, or plotted spectral responses. Such values are marked by the symbol "∼". Values that could not be safely estimated from the available information are indicated as NR.

As shown in Table 2, the proposed hybrid sensor provides a broader analyte-index interval than the earlier Au-only design by extending the lower sensing limit from 1.30 to 1.28. The maximum amplitude sensitivity increases from about 700 RIU^{-1} in the previous Au-only structure [1] to about 842 RIU^{-1} in the present hybrid Au-TiO_2 structure, corresponding to an improvement of approximately 20.3%. This confirms that the TiO_2 overlayer modifies the optical environment around the Au film and strengthens the interaction between the core-guided mode and surface plasmon mode.

The comparison also shows that several reported PCF-SPR sensors achieve high wavelength sensitivity by using side-

polished geometries, D-shaped structures, multi-channel arrangements, or hybrid plasmonic coatings. For example, side-polished and D-type structures improve the access of the guided field to the analyte region, while multi-channel and hybrid-material configurations provide additional degrees of freedom for tailoring the plasmonic response. In contrast, the present design preserves the dual-core PCF sensing platform and introduces an ultra-thin TiO_2 dielectric overlayer as a materials-level modification. This approach improves the modal coupling and extends the usable lower-end refractive-index range without changing the basic sensing architecture.

Although the improvement in amplitude sensitivity is moderate compared with some highly optimized reported designs, the proposed hybrid Au-TiO_2 coating provides a measurable enhancement over the previous Au-only dual-core structure and maintains a stable resonance shift across a relatively wide analyte-index range. Therefore, the contribution of the present work should be interpreted as a parametric hybrid-coating enhancement of a dual-core PCF-SPR architecture rather than a claim of a fundamentally new SPR mechanism.

5. CONCLUSIONS

In this study, a hybrid dual-core PCF-SPR biosensor based on Au and TiO_2 coatings was proposed and numerically investigated using the finite element method. This study was intentionally developed as an extension of our earlier Au-only dual-core PCF-SPR sensor [1], with the main objective of examining how an ultra-thin TiO_2 dielectric overlayer alters the modal coupling condition and overall sensing response. Field-distribution analysis showed that the sensing mechanism is governed by the interaction between the fundamental core-guided mode and plasmonic mode supported at the metal-dielectric interface. Near the phase-matching condition, the modal energy is redistributed from the fiber core toward the coated sensing region, leading to stronger coupling and higher confinement loss. This behavior was clearly reflected in the loss spectra, where the resonance peaks shifted systematically with variations in both structural parameters and analyte refractive index. A detailed parametric analysis demonstrated that the geometrical parameters of the proposed structure, including d_1, d_2, pitch Λ, and dielectric-layer thickness, have a significant influence on the confinement-loss characteristics. By properly tuning these parameters, stronger resonance peaks and improved coupling behavior were obtained, indicating that the hybrid coating provides an additional degree of freedom for optimizing sensor performance. The results further showed that the confinement-loss spectra exhibit a clear redshift as the analyte refractive index increases, confirming the strong dependence of the resonance condition on the surrounding sensing medium. In addition, the amplitude sensitivity was found to increase markedly at higher analyte refractive indices, where the maximum absolute value reached approximately 842 RIU^{-1} at $na = 1.44$, while a similarly high value of about 818 RIU^{-1} was obtained at $na = 1.42$. These results indicate that the proposed sensor becomes more responsive in amplitude interrogation mode in the high-index region. Compared with the previously studied Au-only structure [1], the present Au + TiO_2 design shows a noticeable enhancement in sensing performance. In particular, the maximum absolute amplitude sensitivity is improved from about 700 RIU^{-1} in the previous design to about 842 RIU^{-1} in the present work, corresponding to an enhancement of nearly 20.3%. Furthermore, the analyte refractive-index detection range is extended from 1.30–1.44 to 1.28–1.44, which represents an increase of about 14.3% in the sensing span relative to the previous Au-only design. These quantitative differences confirm the beneficial role of the TiO_2 overlayer in enhancing the sensor response. Overall, the proposed hybrid PCF-SPR biosensor offers improved tunability, stronger amplitude-based response, and a wider usable refractive-index range than the conventional Au-coated configuration. Accordingly, the present study may be regarded as a parametric continuation of our previous Au-only sensor architecture [1], in which the addition of the TiO_2 overlayer provides a practical materials-based route toward higher biosensing performance.

ACKNOWLEDGEMENT

The author acknowledges the University of Kerbala, College of Engineering, for its academic support.

REFERENCES

[1] Naife, R. and A. Abbas, "Induced mode coupling in dual-core photonic crystal for high sensitivity via laser gold film coating," *ARPN Journal of Engineering and Applied Sciences*, Vol. 20, No. 23, 2045–2053, 2025.

[2] Paul, A. K., A. K. Sarkar, M. H. Islam, and M. Morshed, "Dual core photonic crystal fiber based surface plasmon resonance biosensor," *Optik*, Vol. 170, 400–408, 2018.

[3] Wu, T., Y. Shao, Y. Wang, S. Cao, W. Cao, F. Zhang, C. Liao, J. He, Y. Huang, M. Hou, and Y. Wang, "Surface plasmon resonance biosensor based on gold-coated side-polished hexagonal structure photonic crystal fiber," *Optics Express*, Vol. 25, No. 17, 20 313–20 322, 2017.

[4] Candiani, A., S. Giannetti, A. Bertucci, R. M. Naife, H. Al-Janabi, M. Konstantaki, A. Cucinotta, S. Pissadakis, R. Corradini, and S. Selleri, "PNA-modified photonic crystal fibers for DNA detection," in *The European Conference on Lasers and Electro-Optics*, Munich, Germany, May 2013.

[5] Morshed, M., M. I. Hassan, T. K. Roy, M. S. Uddin, and S. M. A. Razzak, "Microstructure core photonic crystal fiber for gas sensing applications," *Applied Optics*, Vol. 54, No. 29, 8637–8643, 2015.

[6] Knight, J. C., "Photonic crystal fibres," *Nature*, Vol. 424, No. 6950, 847–851, 2003.

[7] Russell, P. S. J., "Photonic-crystal fibers," *Journal of Lightwave Technology*, Vol. 24, No. 12, 4729–4749, 2006.

[8] Sharma, A. K., R. Jha, and B. D. Gupta, "Fiber-optic sensors based on surface plasmon resonance: A comprehensive review," *IEEE Sensors Journal*, Vol. 7, No. 8, 1118–1129, 2007.

[9] Hassani, A. and M. Skorobogatiy, "Design criteria for microstructured-optical-fiber-based surface-plasmon-resonance sensors," *Journal of the Optical Society of America B*, Vol. 24, No. 6, 1423–1429, 2007.

[10] Dash, J. N. and R. Jha, "SPR biosensor based on polymer PCF coated with conducting metal oxide," *IEEE Photonics Technology Letters*, Vol. 26, No. 6, 595–598, 2014.

[11] Al Mahfuz, M., M. A. Mollah, M. R. Momota, A. K. Paul, A. Masud, S. Akter, and M. R. Hasan, "Highly sensitive photonic crystal fiber plasmonic biosensor: Design and analysis," *Optical Materials*, Vol. 90, 315–321, 2019.

[12] Ehyaee, A., M. Mohammadi, M. Seifouri, and S. Olyaee, "Design and numerical investigation of a dual-core photonic crystal fiber refractive index sensor for cancer cells detection," *The European Physical Journal Plus*, Vol. 138, No. 2, 129, 2023.

[13] Johnson, P. B. and R. W. Christy, "Optical constants of the noble metals," *Physical Review B*, Vol. 6, No. 12, 4370, 1972.

[14] Lu, Y., C.-J. Hao, B.-Q. Wu, M. Musideke, L.-C. Duan, W.-Q. Wen, and J.-Q. Yao, "Surface plasmon resonance sensor based on polymer photonic crystal fibers with metal nanolayers," *Sensors*, Vol. 13, No. 1, 956–965, 2013.

[15] Ramola, A., A. K. Shakya, V. Kumar, and A. Bergman, "Recent advances in photonic crystal fiber-based SPR biosensors: Design strategies, plasmonic materials, and applications," *Micromachines*, Vol. 16, No. 7, 747, 2025.

[16] Lv, J., J. Wang, L. Yang, W. Liu, H. Fu, P. K. Chu, and C. Liu, "Recent advances of optical fiber biosensors based on surface plasmon resonance: Sensing principles, structures, and prospects," *Sensors & Diagnostics*, Vol. 3, No. 9, 1369–1391, 2024.

[17] Kaziz, S., F. Echouchene, and M. H. Gazzah, "Optimizing PCF-SPR sensor design through Taguchi approach, machine learning, and genetic algorithms," *Scientific Reports*, Vol. 14, No. 1, 7837, 2024.

[18] Yang, Y., Y. Qin, X. Lu, and Y. Zeng, "High-sensitivity three-core photonic crystal fiber sensor based on surface plasmon resonance with gold film coatings," *Japanese Journal of Applied Physics*, Vol. 60, No. 12, 122002, 2021.

[19] Bosch, M. E., A. J. R. Sánchez, F. S. Rojas, and C. B. Ojeda, "Recent development in optical fiber biosensors," *Sensors*, Vol. 7, No. 6, 797–859, 2007.

[20] Saitoh, K. and M. Koshiba, "Numerical modeling of photonic crystal fibers," *Journal of Lightwave Technology*, Vol. 23, No. 11, 3580–3590, 2005.

[21] Cubillas, A. M., S. Unterkofler, T. G. Euser, B. J. M. Etzold, A. C. Jones, P. J. Sadler, P. Wasserscheid, and P. S. J. Russell, "Photonic crystal fibres for chemical sensing and photochemistry," *Chemical Society Reviews*, Vol. 42, No. 22, 8629–8648, 2013.

[22] Ramani, U., H. Kumar, B. K. Singh, and P. C. Pandey, "Design of surface plasmon resonance based both side polished photonic crystal fiber for highly efficient refractive index sensor," *Optik*, Vol. 248, 168062, 2021.

[23] Ying, Y., T. Shang, Z. Gao, and G. Si, "Refractive index sensing characteristics of PCF-SPR based on dual-plasmon materials," *Journal of Optics*, Vol. 26, No. 12, 125101, 2024.

[24] Rifat, A. A., G. A. Mahdiraji, Y. M. Sua, Y. G. Shee, R. Ahmed, D. M. Chow, and F. R. M. Adikan, "Surface plasmon resonance photonic crystal fiber biosensor: A practical sensing approach," *IEEE Photonics Technology Letters*, Vol. 27, No. 15, 1628–1631, 2015.

[25] Hasan, M. S., M. A. E. Kalam, and M. Faisal, "PCF based four-channel SPR biosensor with wide sensing range," *IEEE Transactions on Nanobioscience*, Vol. 23, No. 2, 233–241, 2024.

[26] Sardar, M. R. and M. Faisal, "Numerical analysis of highly sensitive twin-core, gold-coated, D-shaped photonic crystal fiber based on surface plasmon resonance sensor," *Sensors*, Vol. 23, No. 11, 5029, 2023.

[27] Emon, W., A. Chaki, T. P. Mondal, M. F. Nayan, and R. R. Mahmud, "Photonic crystal fiber-based SPR biosensor coated with Ag-TiO_2 and Au-TiO_2 for the detection of skin cancer: A comparison," *Optical and Quantum Electronics*, Vol. 56, No. 8, 1322, 2024.

[28] Ding, X., Q. Lin, M. Wang, S. Liu, W. Zhang, N. Chen, and Y. Wang, "Design and simulation of high-performance D-type dual-mode PCF-SPR refractive index sensor coated with Au-TiO_2 layer," *Sensors*, Vol. 24, No. 18, 6118, 2024.

[29] Jain, S., K. Choudhary, and S. Kumar, "Photonic crystal fiber-based SPR sensor for broad range of refractive index sensing applications," *Optical Fiber Technology*, Vol. 73, 103030, 2022.

[30] Homola, J., "Surface plasmon resonance sensors for detection of chemical and biological species," *Chemical Reviews*, Vol. 108, No. 2, 462–493, 2008.

[31] DeVore, J. R., "Refractive indices of rutile and sphalerite," *Journal of the Optical Society of America*, Vol. 41, No. 6, 416–419, 1951.